Available online at www.sciencedirect.com
SCIENCE DIRECT®
Journal of Solid State Chemistry 177 (2004) 1651–1659
JOURNAL OF SOLID STATE CHEMISTRY
http://elsevier.com/locate/jssc

Crystal structures of disordered $A_2Mn^{3+}M^{5+}O_6$ (A = Sr, Ca; M = Sb, Nb, Ru) perovskites

Michael W. Lufaso,[1] Patrick M. Woodward,* and Joshua Goldberger[2]

Department of Chemistry, Ohio State University, 100 West 18th Ave., Columbus, OH 43210-1173, USA

Received 15 July 2003; received in revised form 8 December 2003; accepted 17 December 2003

Abstract

Polycrystalline samples of A_2MnMO_6 (A = Sr, Ca; M = Nb, Sb, Ru) were prepared by conventional solid state synthesis and their crystal structures were determined using neutron powder diffraction data. All six compounds can be classified as distorted, disordered perovskites. The Mn^{3+}/M^{5+} distribution is disordered in all six compounds. The strontium containing compounds, Sr_2MnMO_6 (M = Nb, Sb, Ru), undergo out of phase rotations of the octahedra about the c-axis (tilt system $a^0a^0c^-$) leading to tetragonal $I4/mcm$ space group symmetry. The calcium containing compounds, Ca_2MnMO_6 (M = Nb, Ru, Sb), have orthorhombic $Pnma$ space group symmetry, as a result of a $GdFeO_3$-type octahedral tilting distortion (tilt system $a^-b^+a^-$). A cooperative Jahn–Teller distortion is observed in Sr_2MnSbO_6 and Sr_2MnRuO_6, but it is much smaller than the distortion observed in $LnMnO_3$ (Ln = lanthanide ion) perovskites. It is possible that Jahn–Teller distortions of the MnO_6 octahedra take place on a short-range length scale in the other four compounds, but there is little or no evidence for cooperative ordering of the local distortions. These findings demonstrate a link between orbital ordering, cation ordering and octahedral tilting.

Keywords: Cooperative Jahn–Teller distortions; Cation ordering; Orbital ordering; Neutron powder diffraction; Perovskites; Octahedral tilting

1. Introduction

The perovskite structure type is one of the most regularly observed structure types in solid state inorganic chemistry. Perovskite oxides with AMO_3 stoichiometry are composed of a three-dimensional framework of corner-sharing MO_6 octahedra. The ability of the corner-sharing octahedral framework to undergo cooperative tilting distortions accounts for the large family of compounds that adopt this structure type. Chemical substitutions can be made on both cation sites as well as the anion site. Cation ordering is common, in $A_2M'MO_6$ compositions, where two different ions occupy the octahedral site in equal concentration [1]. However, the M' and M ions can also adopt a disordered arrangement if the radius and oxidation states of the two ions are similar. Octahedral tilting distortions occur in response to a size mismatch between the A-site cation and the corner sharing octahedral network. These distortions significantly alter the cuboctahedral coordination of the A-site cation, but leave the local octahedral coordination of the M-site cation intact. Octahedral bond distances and angles tend to remain quite symmetric after tilting, provided there is no electronic driving force present to cause a distortion. However, in octahedral coordination the Mn^{3+} cation has the electron configuration $(t_{2g})^3(e_g)^1$. Electronically this is an unfavorable situation and the Jahn–Teller (J–T) theorem states a distortion from octahedral symmetry should occur in order to remove the electronic degeneracy [2]. Such a distortion is experimentally observed in $LnMnO_3$ (Ln = lanthanide ion) perovskites, where the crystal structures show a significant elongation of two Mn–O bonds *trans* to each other. In spite of the bond length reorganization, significant distortions of the O–Mn–O bond angles are not seen in these compounds [3].

While the J–T theorem predicts a distortion of the local coordination environment about octahedral Mn^{3+}

*Corresponding author.
E-mail address: woodward@chemistry.ohio-state.edu (P.M. Woodward).
[1] Current address: Materials Science and Engineering Laboratory, National Institute of Standards and Technology, Gaithersburg, MD 20899, USA
[2] Current address: Department of Chemistry, University of California, Berkeley, Berkeley, CA 94720-1460, USA

0022-4596/$ - see front matter © 2004 Elsevier Inc. All rights reserved.
doi:10.1016/j.jssc.2003.12.020

it does not provide any clues regarding the details of this distortion. In an extended solid these distortions are coupled to each other, so that interactions between octahedra as well as with other ions in the crystal structure can significantly influence the size and type of distortion. This creates the possibility that changes in either the octahedral tilting or the cation order can modify either the local J–T distortion or the long-range order of these distortions. A good example of this can be found in the crystal structures of the disordered perovskites, La_2GaMnO_6 and Nd_2GaMnO_6 [4]. Interestingly, a cooperative Jahn–Teller distortion is present in Nd_2GaMnO_6, whereas no such cooperative distortion is observed in La_2GaMnO_6. Relatively subtle differences in octahedral tilting are proposed to be the source of the unexpectedly distinct crystal chemistry of these two compounds. Investigation of the perovskite series A_2MnMO_6 (A = Ca, Sr; M = Ru, Sb, Nb), in which various degrees of octahedral tilting, cation ordering, and Jahn–Teller distortions are possible may provide additional insight into the coupling between these three distortion mechanisms.

Orbital ordering is a term that has gained favor in recent years. It refers to the preferential occupation of certain atomic orbitals in a crystal. Anisotropic occupation of the e_g orbitals of Mn^{3+} is of course the driving force behind the cooperative Jahn–Teller distortion (CJTD), so that in these compounds the CJTD and orbital ordering are closely, if not inseparably, linked. Determination of accurate crystal structures (particularly the oxygen atom positions) is a necessary first step along the path to constructing a detailed understanding of orbital ordering. Neutron diffraction is a powerful technique for accurate determination of oxygen positions in oxides. Accurate coordination of the octahedral cations can then be extracted from the neutron powder diffraction data using the Rietveld method [5]. Analysis of the crystal structure, focusing on the orientation of the long Mn–O bonds, provides an indirect picture of the orbital occupation and ordering. A search of the literature for accurate A_2MnMO_6 crystal structures reveals several gaps in our knowledge. Accurate structural information was not available for Sr_2MnNbO_6, Sr_2MnSbO_6, Sr_2MnRuO_6, Ca_2MnNbO_6, Ca_2MnSbO_6 and Ca_2MnRuO_6. Consequently, samples of these compounds were synthesized and the structures determined from neutron powder diffraction data in order to better understand the interactions between cation ordering, Jahn–Teller distortions, and octahedral tilting.

2. Experimental

Polycrystalline samples of Sr_2MnNbO_6, Sr_2MnRuO_6, Sr_2MnSbO_6, Ca_2MnNbO_6, Ca_2MnRuO_6 and Ca_2MnSbO_6 were synthesized by standard solid state reaction techniques. Stoichiometric amounts of $CaCO_3$ (Mallincrokdt 99.8%), $SrCO_3$ (MCB 99.7%), Mn_2O_3 (Aldrich 99.9%), Nb_2O_5 (Alfa 99.9%), Sb_2O_3 (Cerac 99.9%), and RuO_2 (Cerac 99.9%) were accurately weighed out and intimately mixed by grinding in an agate mortar and pestle. Reactants were fired in air as a powder in high form alumina crucibles. The crucibles were covered to minimize potential cation volatility at the elevated synthesis temperature. Each sample was reground in an agate mortar and pestle between firings. Sample purity was checked after each heating cycle by X-ray diffraction. Heating cycles continued until the sample attained equilibrium and no change in the weakest peaks could be observed in laboratory X-ray diffraction patterns. Reactants were initially heated to 900–950°C for 10–12 h to decompose the carbonates. Final annealing temperatures and heating/cooling rates were as follows: Sr_2MnNbO_6 (1415°C, 5°C min^{-1}), Sr_2MnRuO_6 (1420°C, 5°C min^{-1}), Sr_2MnSbO_6 (1375°C, 3°C min^{-1}), Ca_2MnMO_6 (M = Sb, Nb, Ru) (1385°C, 3°C min^{-1}). Each polycrystalline sample was dark black in color. After the final annealing cycle, X-ray diffraction data were collected for each sample on a Bruker D8 Advance diffractometer equipped with a Cu X-ray tube, an incident bean Ge (111) monochromator, incident beam Soller slits, and a PSD detector. Data collection proceeded with a 0.0144° 2θ step size in the angular range $15° < 2\theta < 100°$ and a counting time of 2 s. Sample purity and single phase verification was checked by performing Rietveld refinements of the X-ray diffraction data using Topas refinement software [6].

In order to improve the accuracy of the refinement, particularly with regard to the oxygen positions, neutron powder diffraction data were collected at the Australian Nuclear Science and Technology Organisation (ANSTO) under ambient conditions. The wavelength of the medium resolution data collection was 1.32137 Å in the angular range $2.154° < 2\theta < 120°$. Samples (10 g each, except in the case of Ca_2MnRuO_6 where a 7 g sample was used) were analyzed in vanadium containers. In the case of Sr_2MnRuO_6 neutron powder diffraction data were collected using the BT-1 32 detector diffractometer at NIST. A Cu(311) monochromator with a 90° take-off angle, $\lambda = 1.5402(2)$ Å, angular range $3° < 2\theta < 168°$, and in-pile collimation of 15 min of arc was used.

Rietveld structural refinement of the neutron data was carried out using the GSAS [7] program suite as implemented in the EXPGUI interface [8]. Refinements of the X-ray data were carried out using the Topas software package. Initially the lattice parameters, zero point error, scale factor and the background were refined. A 6 (NIST) or 12 (ANSTO) term Chebyschev polynomial was used to model the background. The profile parameters were refined next. The neutron peak

shapes were found to be adequately modeled using either a Gaussian function (ANSTO data) or a pseudo-voigt function (NIST data) to describe the broadening. Finally, the atomic coordinates and isotropic displacement parameters were refined.

3. Expectations and previous structural studies

When the tolerance factor [9] is less than unity an octahedral tilting distortion is expected. Tolerance factors (τ) for the compositions synthesized in this study are calculated assuming an ordered arrangement of M-site cations using the software program SPuDS [10]. Tolerance factors[3] for the three compounds containing strontium are as follows: $Sr_2MnRuO_6 = 0.987$, $Sr_2MnNbO_6 = 0.985$ and $Sr_2MnSbO_6 = 0.977$. Previous studies have shown that when the tolerance factor falls in the 0.97–1.00 range several different octahedral tilting arrangements are competitive, including: $a^-a^-a^-$, $a^-b^0a^-$, $a^0a^0c^-$ and $a^-b^+a^-$ [10,11]. However, when the octahedral sites are occupied by a 50:50 mixture of two different cations, and $A = Sr^{2+}$ the most likely octahedral tilting pattern appears to be $a^0a^0c^-$ [12]. This type of tilting leads to a tetragonal unit cell with $I4/m$ space group symmetry if the Mn/M ions are ordered, and $I4/mcm$ symmetry in the absence of cation order. There is a relatively small contrast between the six coordinate crystal radii of Mn^{3+} (0.79 Å) and the pentavalent ions studied here Nb^{5+} (0.78 Å), Sb^{5+} (0.74 Å) and Ru^{5+} (0.71 Å) [13]. Therefore, a disordered cation distribution ($I4/mcm$ symmetry) is a distinct possibility for the three Sr_2MnMO_6 compounds. Replacing strontium with the smaller calcium ion naturally reduces the tolerance factor: $Ca_2MnRuO_6 = 0.936$, $Sr_2MnNbO_6 = 0.933$ and $Sr_2MnSbO_6 = 0.924$. Tolerance factors in this range almost invariably lead to the $a^-b^+a^-$ octahedral tilting seen in $GdFeO_3$ [14] and $CaTiO_3$ [15]. A $GdFeO_3$-type tilting distortion leads to monoclinic $P2_1/n$ space group symmetry if the Mn/M ions are ordered, and orthorhombic $Pnma$ symmetry for a disordered cation distribution.

There have been several reports in the literature regarding the crystal structures of the compounds investigated in this study. However, these studies have all been based on analysis of laboratory X-ray powder diffraction data and the findings are somewhat at odds with the expectations outlined in the preceding paragraph. These two factors prompted us to revisit the results. The compounds Sr_2MnMO_6 (M = Ta, Nb) were first reported as simple (disordered) cubic perovskites, with cell edges of 3.986 Å (Ta) and 3.959 Å (Nb) [16]. Sr_2MnSbO_6 was reported to be tetragonal ($a = 7.86$ Å, $c = 8.08$ Å) with a disordered arrangement of M-site cations [17]. A magnetic study of Sr_2MnSbO_6 indicated that manganese was present in only one oxidation state, however, this study did not include detailed structural information [18]. Later the structure of Sr_2MnSbO_6 was reported in the obscure (for perovskites) space group $I4mm$ with a final R_{wp} value of 9.1% [19]. Still another study reported Sr_2MnSbO_6 to be a semiconductor ferroelectric with an ordered Mn/Sb arrangement and space group symmetry of $I4mm$ or $I4/mmm$ [20]. The latter study reported an unusual distortion of the MnO_6 octahedron in Sr_2MnSbO_6 with four short, one medium and one long bond [20]. The authors suggest the assignment of the oxygen positions may differ significantly from the value reported, due to the difficulty in refining accurate fractional coordinates for the oxygen atoms from laboratory powder X-ray data. Furthermore, it is hard to see what electronic driving force would stabilize a rarely observed 4+1+1 type of octahedral distortion. The structure of Sr_2MnRuO_6 has been reported as monoclinic, but the evidence to support such an assignment is not clear [21]. It was earlier found [12] from analysis of laboratory powder X-ray diffraction data that both Sr_2MnSbO_6 and Sr_2MnTaO_6 belong to the tetragonal space group $I4/mcm$. The structure of Ca_2MnNbO_6 was reported in space group $Pbnm$, a non-standard setting of $Pnma$ [22], consistent with a disordered Mn/Nb distribution and $a^-b^+a^-$ octahedral tilting.

4. Results

The X-ray and neutron diffraction patterns of all three strontium containing compounds could be indexed using a tetragonal unit cell with dimensions $a \cong \sqrt{2}a_p$ and $c \cong 2a_p$, where a_p is the ideal primitive cubic perovskite lattice parameter. The reflection conditions observed in the diffraction pattern are in agreement with those expected for space group $I4/mcm$ (among others). The presence of a c-glide plane perpendicular to the b-axis is a strong indicator of the lack of Mn/M cation order. The intensities of the 1 0 1 and 0 1 1 peaks (the 1 1 1 peak in the doubled pseudo-cubic cell) in both the X-ray and neutron diffraction patterns are particularly sensitive to changes in cation order. The absence of these peaks in all of patterns collected is further proof of a disordered cation arrangement. Nonetheless, the possibility of cation order was not completely dismissed at this stage of the analysis.

Due to the various conflicting reports regarding the space group symmetry and cation order for these

[3] Tolerance factors were calculated using SPuDS software, which calculates the tolerance factor by calculating the M–O and A–O distances that results in bond valence sums equal to the formal oxidation state assuming 6 and 12-fold symmetric coordination for the M and A-site cations, respectively. The M–O and A–O bond distances are then used in the tolerance factor equation $\tau = d(A-O)/2d(M-O)$.

compounds, refinements of the X-ray and neutron data were undertaken using a variety of models. Space groups $I4mm$ and $I4/mmm$ were attempted using a fully ordered Mn/M distribution and the atomic coordinates from [19] as a starting model. A model based upon a fully ordered cation distribution in combination with $a^0a^0c^-$ tilting (space group $I4/m$) was constructed using SPuDS and used to fit the data. All three of these attempts were unsuccessful due in large part to the strong overestimation of the intensity of the peaks that derive their intensity from the cation ordering. This is illustrated for neutron powder data of Sr_2MnNbO_6 in Fig. 1. A disordered $I4mm$ model was attempted and the order of the M-site refined, as was an $I4/mcm$ model where the space group symmetry dictates a disordered cation arrangement. The $I4/mcm$ structural model of Sr_2MnMO_6 (M = Nb, Sb) was generated using SPuDS. Table 1 shows goodness of fit parameters obtained for each compound from the various models and data sets. This table shows how difficult it is to distinguish between the two disordered models from the X-ray data, whereas, the neutron data clearly confirms the $I4/mcm$ model ($R_{wp} = 3.09\%$) as superior to the $I4mm$ model ($R_{wp} = 5.49\%$). In particular the intensities of the 112 and 200 reflections were not reproduced accurately using the $I4mm$ model. Fig. 2 shows the calculated fit of the $I4/mcm$ model to the experimental neutron powder diffraction data. In the $I4/mcm$ model, the atomic positions are as follows: $A(4b)$ $(0, \frac{1}{2}, \frac{1}{4})$, Mn/$M(4c)$ (0, 0, 0), O($4a$) $(0, 0, \frac{1}{4})$, O($8h$) $(x, x+\frac{1}{2}, 0)$. Rietveld refinement results of neutron diffraction data are detailed in Table 2. The crystal structure of Sr_2MnSbO_6 shown in Fig. 3 illustrates the cooperative out-of-phase octahedral tilting about the c-axis.

The space group assignments for the calcium analogues are less ambiguous. Based on tolerance factor considerations given in Section 3, $a^-b^+a^-$ octahedral tilting is expected. Based on the lack of cation order in the strontium compounds, it is reasonable to expect the calcium series will also be disordered perovskites. Close inspection of the peaks that owe their intensity primarily to cation order confirms this assumption. The structural models for all three compounds were generated using

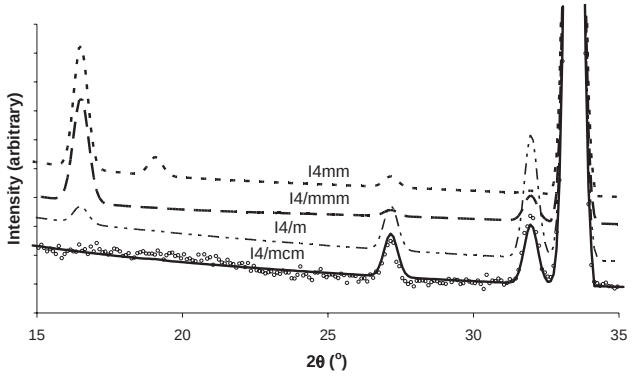

Fig. 1. Models based on space groups $I4mm$ and $I4/mmm$ (fully ordered Mn/M distribution) and space group $I4/m$ display a strong overestimation of the intensity of the peaks that derive their intensity from the cation ordering in the Sr_2MnNbO_6 neutron powder diffraction data.

Table 1
Goodness of fit parameters for refinements of Sr_2MnMO_6 (M = Nb, Ru, Sb) structures using X-ray and neutron data

Space group	$I4/mmm$	$I4/m$	$I4mm$	$I4mm$	$I4/mcm$
Cation order parameter	100%	100%	100%	0%	0%
Octahedral tilting	None	$a^0a^0c^-$	None	None	$a^0a^0c^-$
Sr_2MnNbO_6 X-ray R_{wp} (%)	6.02	6.36	6.24	3.45	3.22
Sr_2MnNbO_6 neutron R_{wp} (%)	8.12	5.87	8.66	8.02	3.72
Sr_2MnSbO_6 X-ray R_{wp} (%)	13.69	12.49	13.82	5.55	5.17
Sr_2MnSbO_6 neutron R_{wp} (%)	6.62	6.20	8.60	8.63	3.09
Sr_2MnRuO_6 neutron R_{wp} (%)	22.13	12.07	23.06	17.32	6.63

The structural models are described in the text.

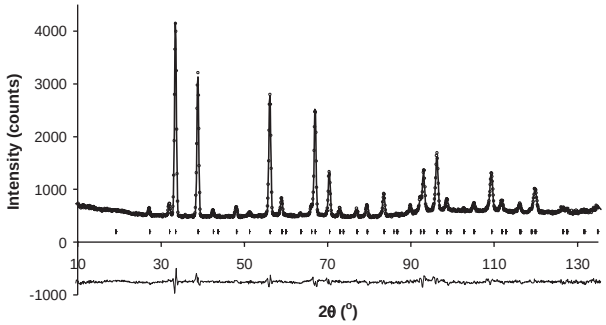

Fig. 2. Observed (circles), calculated (line) and difference (bottom) patterns for the neutron powder diffraction data set collected for Sr_2MnNbO_6 and refined using the $I4/mcm$ model.

Table 2
Refinement results for Sr_2MnMO_6 (M = Nb, Ru, Sb) based on neutron powder diffraction data

Compound	Sr_2MnNbO_6	Sr_2MnRuO_6	Sr_2MnSbO_6
R_p (profile)	2.91	5.12	2.48
R_{wp} (weighted profile)	3.73	6.63	3.09
Reduced χ^2	4.01	1.33	2.43
Number of reflections	112	82	111
Total refined variables	24	23	24
Space group	$I4/mcm$ (♯140)	$I4/mcm$ (♯140)	$I4/mcm$ (♯140)
a (Å)	5.6119(6)	5.45459(1)	5.5553(2)
c (Å)	7.927(1)	7.9340(2)	8.0548(3)
Volume (Å^3)	249.65(2)	236.16(1)	248.58(2)
O2 x	0.2248(4)	0.2199(1)	0.2200(3)
Sr U_{Iso} (Å$^2 \times 100$)	1.63(6)	0.99(3)	1.41(8)
Mn/M U_{iso} (Å$^2 \times 100$)	0.4(1)	0.70(7)	−0.5(2)
O1 U_{iso} (Å$^2 \times 100$)	2.4(2)	[a]	2.1(1)
O2 U_{iso} (Å$^2 \times 100$)	1.28(6)	[a]	1.40(5)

[a] Anisotropic displacement parameters were used to model oxygen. The refined U (Å$^2 \times 100$) values were as follows, O1: $U_{11} = U_{22} = 1.25(4)$, $U_{33} = 1.44(8)$; O2: $U_{11} = U_{22} = 0.89(2)$, $U_{33} = 1.48(5)$, $U_{12} = 0.54(4)$.

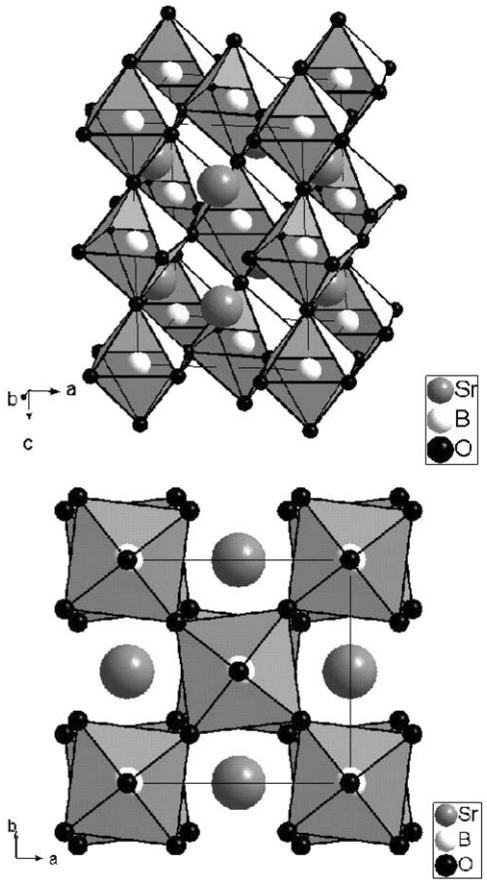

Fig. 3. Crystal structure of Sr_2MnSbO_6. Large spheres represent Sr. Small dark spheres represent O and a random distribution of *B*-site cations Mn and Nb are represented by the white spheres.

SPuDS and assuming a disordered *M*-site *Pnma* perovskite structure, with symmetric *M*–O bond distances. The atomic positions are as follows: *A*(4*c*) $(x, \frac{1}{4}, z)$, Mn/*M*(4*b*) $(\frac{1}{2}, 0, 0)$, O1(4*c*) $(x, \frac{1}{4}, z)$, O2(8*d*) (*x*, *y*, *z*). The Rietveld refinement results, based on the neutron diffraction data, are detailed in Table 3. Refined fits to the diffraction patterns are shown in Fig. 4. The crystal structure of Ca_2MnSbO_6 shown in Fig. 5 illustrates the in-phase tilting of the octahedra perpendicular along the *b*-axis and the out of phase tiltings in the *ac* plane of space group *Pnma*.

The complex redox chemistry of manganese raises the possibility for non-stoichiometry. In previous studies, oxygen non-stoichiometry was observed in Ca_2MnNbO_γ ($5.86 < \gamma < 6.00$) depending upon post-reaction heat treatment at different oxygen pressures on a high-temperature quenched sample [22]. High O_2 pressures were observed to give $\gamma = 6.00$, while final heat treatments in air at 1400°C resulted in $\gamma = 5.87$. In this compound lattice parameters showed little change in *a* and *b*, with a small increase in *c* with decreasing γ. Linear interpolation and use of the lattice parameter observed in the neutron data used in this study results in an estimated $\gamma = 5.91$ and X-ray data results in an estimated $\gamma = 5.88$ for the sample synthesized at 1385°C. These values are in very good agreement with the earlier study. The cooling profile utilized in this study is expected to increase the O content slightly towards the fully stoichiometric composition, which reached a maximum of $\gamma = 5.94$ for annealing at 400°C in air [22]. Rietveld refinement of neutron powder diffraction data is an additional technique that is sensitive to oxygen vacancies. Refinement of the occupancies, $f[O(4c)] = 1.01(2)$ and $f[O(8d] = 1.00(1)$, of the oxygen sites did not lead to any significant deviation from full site occupancy. In conclusion, while we cannot completely rule out oxygen non-stoichiometry, the deviation from the ideal stoichiometry is small.

Table 3
Refinement results for Ca_2MnMO_6 (M = Nb, Ru, Sb) based on neutron powder diffraction data

Compound	Ca_2MnNbO_6	Ca_2MnRuO_6	Ca_2MnSbO_6
R_p (profile)	2.14	2.42	2.35
R_{wp} (weighted profile)	2.60	2.92	2.85
Reduced χ^2	2.80	2.37	1.99
Number of reflections	449	415	447
Total refined variables	31	31	31
Space group	*Pnma* (♯62)	*Pnma* (♯62)	*Pnma* (♯62)
a (Å)	5.5635(4)	5.4207(3)	5.5549(5)
b (Å)	7.6996(5)	7.5757(4)	7.6941(6)
c (Å)	5.4530(4)	5.3346(3)	5.4591(4)
Volume (Å^3)	233.59(4)	219.07(2)	233.32(4)
Ca *x*	0.5459(6)	0.5425(5)	0.5469(9)
Ca *z*	0.5100(9)	0.5058(9)	0.511(1)
O1 *x*	−0.0226(4)	−0.0181(4)	−0.0257(6)
O1 *z*	0.4175(5)	0.4208(5)	0.4135(7)
O2 *x*	0.2947(3)	0.2939(3)	0.2942(5)
O2 *y*	0.0425(2)	0.0398(2)	0.0434(3)
O2 *z*	0.7039(3)	0.7050(3)	0.7031(5)
Ca U_{iso} (Å$^2 \times 100$)	1.53(7)	0.69(5)	1.58(9)
Mn/M U_{iso} (Å$^2 \times 100$)	0.0(1)	0.7(1)	0.4(4)
O1 U_{iso} (Å$^2 \times 100$)	1.03(6)	0.66(5)	1.03(8)
O2 U_{iso} (Å^2 $\times 100$)	1.02(4)	0.46(3)	1.16(6)

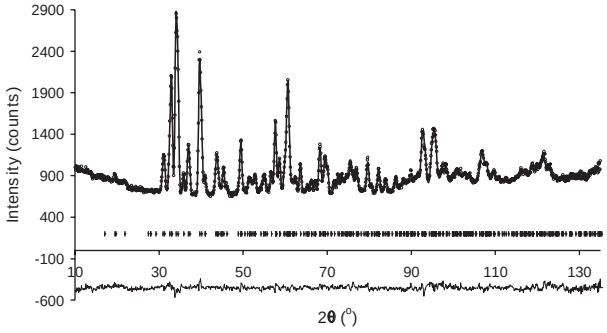

Fig. 4. Observed (circles), calculated (line) and difference (bottom) patterns for the neutron powder diffraction data set collected for Ca_2MnNbO_6 and refined using the *Pnma* model.

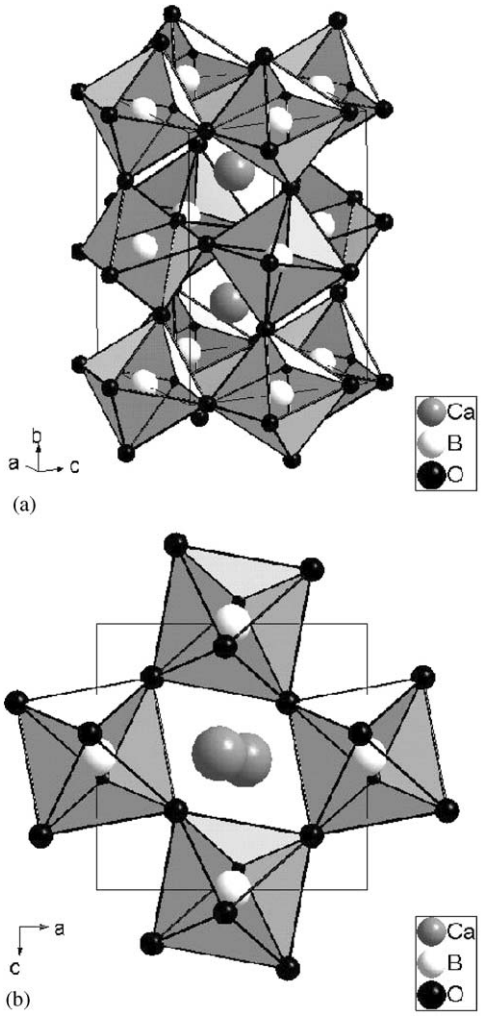

Fig. 5. Crystal structure of Ca_2MnSbO_6. Large spheres represent Ca. Small dark spheres represent O and a random distribution of *B*-site cations Mn and Sb are represented by the white spheres.

5. Discussion

Selected bond distances, bond angles, and bond valence sums are shown in Tables 4 and 5. Bond valence sums for Sr^{2+} and Ca^{2+} are very close to their ideal values, confirming the accuracy with which the octahedral tilting distortions have been determined. Valence sums for the Mn^{3+} and M^{5+} ions show some deviation from their ideal values. However, it should be kept in mind that due to the cation disorder the bond distances extracted from the refinement represent an average of various local environments. In such instances it is expected that the bond valence sums will deviate somewhat from their ideal values. Table 6 gives the crystallographic parameters predicted by SPuDS for each compound. The good agreement between the oxygen fractional coordinates and the Mn–O–*M* angles predicted by SPuDS and those determined experimentally is consistent with previous demonstrations of the accuracy of the program [10]. Deviations between the predicted and observed unit cell parameters originate primarily in distortions of the octahedra, including cooperative Jahn–Teller distortions.

The bond distances shown in Table 4 reveal a nearly symmetric coordination environment for the *M*-site ions in the $Ca_2Mn\mathit{M}O_6$ (M = Nb, Ru, Sb) series. The same can be said for the Nb–O bond distances listed in Table 5 for Sr_2MnNbO_6. It is also worth pointing out that unit cell volumes observed for Ca_2MnSbO_6 and Ca_2MnNbO_6 are nearly identical, as are those for Sr_2MnSbO_6 and Sr_2MnNbO_6. The implication is that the ionic radius of Sb^{5+} is nearly the same as Nb^{5+}. This is somewhat in contradiction to the differing predictions of ionic radii, Nb–O dist. = 1.99 Å, Sb–O dist. = 1.95 Å, [14] and bond valence summations, Nb–O dist. = 1.98 Å, Sb–O dist. = 2.01 Å [23,24]. Apparently the Nb^{5+} radius is well established, but there is a lack of agreement regarding the Sb^{5+} radius. The similarity between the radii of Nb^{5+} and Sb^{5+} is supported not only by this study, but also by previous crystal structure determinations of ordered double perovskites containing Sb^{5+}. Examples include Sr_2FeSbO_6 [25], Ba_2TlSbO_6 [26], Ba_2BiSbO_6 [27] and La_2LiSbO_6 [28], where the mean Sb–O distances are 1.98, 1.98, 1.987, and 1.986 Å, respectively. The unit-cell volumes and *M*–O distances of Ca_2MnRuO_6 and Sr_2MnRuO_6 are noticeably smaller than the Nb and Sb analogues. Once again an inspection of the literature of ruthenium containing perovskites is illustrative. Battle and co-workers have examined a large number of ordered $A_2M\mathrm{Ru}^{5+}O_6$ perovskites and found consistently that the average Ru^{5+}–O distance falls in the range 1.95–1.96 Å [29–31]. Given this value and the expectation that the Mn^{3+}–O distance should fall in the range 1.99–2.00 Å [14], one would expect the average Mn/Ru distance to be ~1.97 Å. Yet in both A_2MnRuO_6 the average distance is somewhat smaller, ~1.95 Å. This deviation from expectations could arise from a small amount of electron transfer from Mn^{3+} to Ru^{5+}. Stated in another way there could be some measure of mixing between the Mn^{3+}/Ru^{5+} and the Mn^{4+}/Ru^{4+} oxidation state couples. Partial evidence for this hypothesis comes from the report that Sr_2MnRuO_6 is reasonably good electronic conductor $\sigma_{300K} \sim 40\,\Omega^{-1}\,cm^{-1}$ [32].

In contrast to the compounds discussed in the preceding paragraph, both Sr_2MnSbO_6 and Sr_2MnRuO_6 show a small but significant elongation of the Mn/*M*–O bonds parallel to the *c*-axis. Particularly noteworthy is the contrast between the very similar structures of Ca_2MnSbO_6 and Ca_2MnNbO_6 with the somewhat differing structures of Sr_2MnSbO_6 and Sr_2MnNbO_6. This comparison clearly brings out the presence of a cooperative Jahn–Teller distortion and the corresponding orbital ordering in Sr_2MnSbO_6 and Sr_2MnRuO_6. The CJTD is the origin of SPuDS underestimation of the length of the tetragonal *a*-axis. It should be noted

Table 4
Selected bond distances and bond valence sums for Ca_2MnMO_6 (M = Nb, Ru, Sb) from refinements of neutron powder diffraction data

		Ca_2MnNbO_6	Ca_2MnRuO_6	Ca_2MnSbO_6
Mn/*M*–O bond distances (Å)	*M*–O(4*c*) × 2	1.9807(7)	1.9429(6)	1.9858(9)
	M–O(8*d*) × 2	2.005(2)	1.953(2)	2.011(3)
	M–O(8*d*) × 2	2.008(2)	1.956(2)	2.003(3)
	Mean *M*–O	1.998	1.951	2.000
Ca–O bond distances (Å)	Ca–O(4*c*)	3.202(4)	3.073(4)	3.225(6)
	Ca–O(4*c*)	2.453(4)	2.424(4)	2.433(6)
	Ca–O(4*c*)	2.362(5)	2.299(5)	2.352(7)
	Ca–O(4*c*)	3.145(5)	3.076(5)	3.168(7)
	Ca–O(8*d*) × 2	2.371(4)	2.341(3)	2.366(5)
	Ca–O(8*d*) × 2	2.687(3)	2.621(3)	2.691(4)
	Ca–O(8*d*) × 2	2.627(4)	2.603(4)	2.617(5)
M–O–*M* angles (°)	*M*–O(4*c*)–*M*	152.7(2)	154.2(2)	151.2(2)
	M–O(8*d*)–*M*	152.2(1)	153.19(9)	151.9(1)
Bond valence sums (v.u.)	Ca^{2+}	1.98	2.23	2.02
	Mn^{3+}	3.16	3.58	3.14
	M^{5+}	4.75	5.23	5.13
	$O(4c)^{2-}$	2.09	2.30	2.14
	$O(8d)^{2-}$	1.93	2.17	2.01

Bond valence sums were calculated with SPuDS using bond distances obtained from the refinements from neutron data. Bond valence parameters used were as follows: $R_{Ca-O} = 1.967$, $R_{Nb-O} = 1.911$, $R_{Ru-O} = 1.90$, $R_{Sb-O} = 1.942$ and $B = 0.37$ in each case.

Table 5
Selected bond distances and bond valence sums for Sr_2MnMO_6 (M = Nb, Ru, Sb) from the refinements of neutron powder diffraction data

		Sr_2MnNbO_6	Sr_2MnRuO_6	Sr_2MnSbO_6
Mn/*M*–O bond distances (Å)	*M*–O(4*a*) × 2	1.9818(4)	1.98349(4)	2.0137(1)
	M–O(8*h*) × 4	1.9937(4)	1.9429(1)	1.9781(3)
Mean Mn/*M*–O (Å)	*M*–O	1.990	1.957	1.990
Sr–O bond distances (Å)	Sr–O(4*a*) × 4	2.8060(3)	2.6100(5)	2.7777(1)
	Sr–O(8*h*) × 4	2.670(2)	2.72795(5)	2.653(1)
	Sr–O(8*h*) × 4	2.946(2)	2.9337(6)	2.982(2)
M–O–*M* angles (°)	*M*–O(4*a*)–*M*	180	180	180
	M–O(8*h*)–*M*	168.7(2)	166.25(5)	166.3(1)
Bond valence sums (v.u.)	Sr^{2+}	1.95	2.27	2.00
	Mn^{3+}	3.23	3.53	3.23
	M^{5+}	4.85	5.16	5.28
	$O(4a)^{2-}$	2.00	2.11	2.00
	$O(8h)^{2-}$	1.99	2.25	2.13

Bond valence sums were calculated with SPuDS using bond distances obtained from the refinements from neutron data. Bond valence parameters used were as follows: $R_{Sr-O} = 2.118$, $R_{Nb-O} = 1.911$, $R_{Ru-O} = 1.90$, $R_{Sb-O} = 1.942$ and $B = 0.37$ in each case.

that this distortion is much smaller than the cooperative J–T distortion seen across the LnMnO$_3$ perovskite series [3]. The reduction in the magnitude of the distortion can be attributed in part to dilution effects associated with randomly distributing a symmetric ion (Sb/Ru) and a J–T distorted ion (Mn^{3+}) on the same crystallographic site, but even after this has been taken into consideration, the distortion is considerably smaller than expected based upon extrapolation from the LnMnO$_3$ perovskites.

It is interesting to note the undulating shape of the backgrounds present in the neutron patterns. Backgrounds of this type are characteristic of short-range correlations [33]. These could originate both from

Table 6
SPuDS optimized lattice parameters and free fractional coordinates for A_2MnMO_6 (A = Sr, Ca; M = Nb, Ru, Sb

A	Ca	Ca	Ca	Sr	Sr	Sr
M	Nb	Ru	Sb	Nb	Ru	Sb
a (Å)	5.5619	5.5472	5.6040	5.5943	5.5866	5.6159
b (Å)	7.7512	7.7367	7.7922	—	—	—
c (Å)	5.4073	5.4008	5.4256	7.9727	7.9464	8.0484
Volume (Å^3)	233.12	231.78	236.92	249.52	248.00	253.83
Ca(x)	0.5450	0.5425	0.5519	—	—	—
Ca(z)	0.5148	0.5139	0.5175	—	—	—
O1(x)	−0.0137	−0.0130	−0.0157	0.2189	0.2230	0.2089
O1(z)	0.4149	0.4171	0.4086	—	—	—
O2(x)	0.2902	0.2893	0.2928	—	—	—
O2(y)	0.0426	0.0414	0.0457	—	—	—
O2(z)	0.7074	0.7086	0.7043	—	—	—
M–O distance (Å)	1.993	1.987	2.012	1.993	1.987	2.012
M–O(4)–M angle (°)	152.92	153.61	151.01	180	180	180
M–O(8)–M angle (°)	153.61	153.96	151.46	165.80	167.69	161.35

M/Mn disorder and local J–T distortions that are larger than suggested by the crystallographic structures. These details are discussed in greater detail in a subsequent paper [34].

6. Conclusions

Samples of Sr_2MnMO_6 (M = Nb, Sb, Ru) and Ca_2MnMO_6 (M = Nb, Sb, Ru) were synthesized and their crystal structures determined from neutron powder diffraction data using the Rietveld method. Diffraction peaks associated with M-site cation order were not observed in either the X-ray or neutron powder diffraction data, consistent with the absence of long range Mn/M cation order. Fractional positions of structures generated in the software program SPuDS were used as starting positions in the Rietveld refinements. These values were found to agree well with the final refined fractional coordinates. Octahedral tilting about a single axis ($a^0a^0c^-$) occurs for Sr_2MnMO_6 (M = Nb, Sb, Ru), whereas octahedral tilting about multiple axes ($a^-b^+a^-$) occurs for Ca_2MnMO_6 (M = Nb, Sb, Ru). These findings are in-line with expectations based on the geometric tolerance factors. Sr_2MnSbO_6 and Sr_2MnRuO_6 exhibit a small but unmistakable cooperative Jahn–Teller distortion, with the long Mn–O bonds orienting preferentially parallel to the c-axis. This type of Jahn–Teller distortion is normally observed in ordered perovskites, such as Sr_2CuWO_6 [35], implying either one-dimensional or medium range Mn^{3+}/M^{5+} cation order. The lack of a cooperative Jahn–Teller distortion in the other four compounds studied suggests that changes in either short-range cation order/disorder effects (Sr_2MnNbO_6) or octahedral tilting (Ca_2MnSbO_6 and Ca_2MnRuO_6) or both (Ca_2MnNbO_6) can disrupt the coherency of the orbital ordering.

Acknowledgments

We acknowledge Brett Hunter for neutron powder diffraction data collection at the Australian Nuclear Science and Technology Organisation, Australia. We acknowledge the support of the National Institute of Standards and Technology, US Department of Commerce, in providing the neutron research facilities used in this work. MWL would like to thank the International Centre for Diffraction Data (ICDD) for the 2002 Ludo Frevel Crystallography scholarship. PMW would like to acknowledge the National Science Foundation, grant number ♯DMR-0094271 for financial support.

References

[1] M.T. Anderson, K.B. Greenwood, G.A. Taylor, K.R. Poeppelmeier, Prog. Solid State Chem. 22 (1993) 197.
[2] (a) J. Kanamori, J. Appl. Phys. 31 (1960) 14S.
(b) J.B. Goodenough, Phys. Rev. 100 (1955) 564.
[3] J.A. Alonso, M.J. Martinez-Lope, M.T. Casais, M.T. Fernandez-Diaz, Inorg. Chem. 39 (2000) 917.
[4] E.J. Cussen, M.J. Rosseinski, P.D. Battle, J.C. Burley, L.E. Spring, J.F. Vente, S.J. Blundell, A.I. Coldea, J. Singleton, J. Am. Chem. Soc. 123 (2001) 1111.
[5] H.M. Rietveld, J. Appl. Crystallogr. 2 (1969) 65.
[6] Bruker AXS, 2000—User Manual, Bruker AXS, Karlsruhe, Germany.
[7] A.C. Larson, R.B. von-Dreele, General Structure Analysis System (GSAS), Los Alamos National Laboratories, 1990.
[8] B.J. Toby, Appl. Crystallogr. 34 (2001) 210.
[9] V.M. Goldschmidt, Naturwissenschaften 14 (1926) 477.
[10] M.W. Lufaso, P.M. Woodward, Acta Crystallogr. B 57 (2001) 725.
[11] P.M. Woodward, Acta Crystallogr. B 53 (1997) 44.
[12] P.M. Woodward, Ph. D. Dissertation, Oregon State University, Corvallis, OR, 1997.
[13] R.D. Shannon, Acta Crystallogr. A 32 (1976) 751.
[14] M. Marezio, J.P. Remeka, P.D. Dernier, Acta Crystallogr. B 26 (1970) 2008.

[15] S. Sasaki, C.T. Prewitt, J.D. Bass, Acta Crystallogr. C 43 (1987) 1668.
[16] M.F. Kupriyanov, V.S. Filip'ev, Sov. Phys. Crystallogr. 8 (1963) 278.
[17] G. Blasse, J. Inorg. Nucl. Chem. 27 (1965) 993.
[18] B.Y. Brach, N.P. Bobrysheva, N.V. Chezhina, Russ. J. Inorg. Chem. 27 (1982) 1395.
[19] E.D. Politova, G.M. Kaleva, I.N. Danilenko, V.F. Chuprakov, S.A. Ivanov, N.Y. Venevtsev, Iz. Akad. Nauk SSSR, Neorg. Mater. 26 (1990) 2352.
[20] M.C. Foster, R.M. Nielson, S.C. Abrahams, J. Appl. Phys. 82 (1997) 3076.
[21] M. Fang, M. Kato, K. Yoshimura, K. Kosuge, J. Alloys Compd. 317 (2001) 136.
[22] A. Kruth, M. Tabuchi, U. Guth, A.R. West, J. Mater. Chem. 8 (1998) 2515.
[23] I.D. Brown, D. Altermatt, Acta Crystallogr. B 41 (1985) 244.
[24] I.D. Brown, www.ccp14.ac.uk/ccp/web-mirrors/i_d_brown, Accumulated Table of Bond Valence Parameters, Version 2.2.
[25] E.J. Cussen, J.F. Vente, P.D. Battle, T.C. Gibb, J. Mater. Chem. 7 (1997) 459.
[26] W.T. Fu, D.J.W. Ijdo, J. Solid State Chem. 128 (1997) 323.
[27] W.T. Fu, R. de Gelder, R.A.G. de Graaff, Mater. Res. Bull. 32 (1997) 657.
[28] M.L. Lopez, M.L. Veiga, J. Rodriguez-Carvajal, F. Fernandez, A. Jerez, C. Pico, Mater. Res. Bull. 27 (1992) 647.
[29] P.D. Battle, J.B. Goodenough, R. Price, J. Solid State Chem. 46 (1983) 234.
[30] P.D. Battle, W.J. Macklin, J. Solid State Chem. 52 (1984) 138.
[31] P.D. Battle, C.W. Jones, F. Studer, J. Solid State Chem. 90 (1991) 302.
[32] J. Goldberger, P.N. Santhosh, P.M. Woodward, P.M.P. Karen, A.R. Moodenbaugh, Chem. Mater. (2004), submitted for publication.
[33] M.R. Palacin, J. Bassas, J. Rodriguez-Carvajal, P. Gomez-Romero, J. Mater. Chem. 3 (1993) 1171.
[34] M.W. Lufaso, P.M. Woodward, Acta Crystallogr. B 60 (2004) 10.
[35] D. Iwanaga, Y. Inaguma, M. Itoh, J. Solid State Chem. 147 (1999) 291.